

Acoustic emission source location and noise cancellation for crack detection in rail head

K.S.C. Kuang^a, D. Li^{*} and C.G. Koh^b

Department of Civil and Environmental Engineering, National University of Singapore, 117576, Singapore

(Received December 3, 2015, Revised July 10, 2016, Accepted July 27, 2016)

Abstract. Taking advantage of the high sensitivity and long-distance detection capability of acoustic emission (AE) technique, this paper focuses on the crack detection in rail head, which is one of the most vulnerable parts of rail track. The AE source location and noise cancellation were studied on the basis of practical rail profile, material and operational noise. In order to simulate the actual AE events of rail head cracks, field tests were carried out to acquire the AE waves induced by pencil lead break (PLB) and operational noise of the railway system. Wavelet transform (WT) was first utilized to investigate the time-frequency characteristics and dispersion phenomena of AE waves. Here, the optimal mother wavelet was selected by minimizing the Shannon entropy of wavelet coefficients. Regarding the obvious dispersion of AE waves propagating along the rail head and the high operational noise, the wavelet transform-based modal analysis location (WTMAL) method was then proposed to locate the AE sources (i.e. simulated cracks) respectively for the PLB-induced AE signals with and without operational noise. For those AE signals inundated with operational noise, the Hilbert transform (HT)-based noise cancellation method was employed to improve the signal-to-noise ratio (SNR). Finally, the experimental results demonstrated that the proposed crack detection strategy could locate PLB-simulated AE sources effectively in the rail head even at high operational noise level, highlighting its potential for field application.

Keywords: rail head; crack detection; acoustic emission; source location; noise cancellation; wavelet transform; Hilbert transform

1. Introduction

Condition monitoring of railway system aims to identify defects in advance in order to ensure safe and smooth operation. For the sake of more efficient rail crack detection, various ultrasonic and electromagnetic non-destructive testing (NDT) techniques are under research, one of which is the acoustic emission (AE) (Barke and Chiu 2005, Papaelias *et al.* 2008). AE refers to the generation of transient stress waves produced by the sudden release of elastic strain energy during processes of crack, fracture, impact and so on. Compared with other ultrasonic NDTs, AE technique is more sensitive to crack initiation and propagation, less influenced by the structural geometry and more capable of long-distance crack detection (Ono 2007). It has been successfully

*Corresponding author, Ph.D. Student, E-mail: lidan@u.nus.edu

^a Assistant Professor, Email: ceeksck@nus.edu.sg

^b Professor, E-mail: cgkoh@nus.edu.sg

used for on-line continuous monitoring of structures from rolling bearings to bridges (Li *et al.* 2015, Nair and Cai 2010, Pandya *et al.* 2013), while its application to rail tracks is still limited to laboratory studies using small-scale test rigs. Bruzelius and Mba (2004) demonstrated the potential applicability of AE technique to rail defect detection through AE activities simulated by pencil lead break (PLB) and induced by progressive wear of the track. Thakkar *et al.* (2010) derived a simplified analytical model to describe the expected rolling background noise, and a method to detect surface defects by identifying AE peaks above the normal background. Zhang *et al.* (2015) examined the rolling noise resulting from the test rig at high wheel speeds, and proposed to detect the PLB simulated defects using the time-Shannon entropy of wavelet coefficients. They also studied the features of simulated AE sources with different propagation distances, types and depths on a short segment of steel rail (Zhang *et al.* 2014). However, little attention has been paid to the propagation characteristics and source location of crack-induced AE waves along the rail and the influence of operational noise on crack detection in the railway field.

This paper focuses on the crack detection in rail head, which is one of the most vulnerable parts of rail track (Esveld 2001). It is significant to investigate the source location and noise cancellation methods through field tests. Locating the AE source (i.e., crack) in rail head can be treated as a one-dimensional problem in a homogeneous material. Nonetheless, due to the complicated geometry and high operational noise of rail track, it is not an easy task to precisely determine the arriving time and propagation velocity of AE wave. Especially, when propagating along the rail head, the AE wave should be regarded as guided wave (Coccia *et al.* 2011), of which the key feature is velocity dispersion. The dispersion phenomena of AE wave, if not being taken care of, would bring errors in the source location results. There have been many researches on AE source location in plate structures using the dispersive Lamb wave modes through modal analysis (Ciampa and Meo 2010, Hamstad *et al.* 2002, Holford *et al.* 2001). However, it needs to be further studied for crack detection in rail head, where the Rayleigh-Lamb equation does not apply, and the frequency characteristics of crack-induced AE wave and operational noise are unknown.

There are two main approaches of AE source location: time-of-arrival (TOA) method, which relies on the time difference between arrivals of an individual AE event at two adjacent sensors, and single sensor modal analysis location (SSMAL) method, which makes use of the time delay between two dispersive wave modes at one sensor (Ernst and Dual 2014). If wavelet transform (WT) is applied to analyze the dispersive wave modes (Jiao *et al.* 2008, Takemoto *et al.* 2000), the SSMAL method can be named as wavelet transform-based modal analysis location (WTMAL) method. The WTMAL method is proposed to locate rail head cracks in this paper for two reasons. First, AE waves exhibit obvious dispersion when propagating along the rail head. Being aware of the wave dispersion phenomena, the WTMAL method is more accurate than the TOA method, where the wave velocity used is actually the average velocity of various dispersive wave modes. Second, when a wheel is too close to the sensor, the operational noise caused by wheel-rail interaction may obscure the crack-induced AE signal aroused by another wheel far away due to the energy attenuation. The WTMAL method requires only one sensor to determine the distance between AE source and sensor, and is thus less susceptible to the operational noise compared to the TOA method.

In this paper, an AE strategy for crack detection in rail head, comprising a source location method and a noise cancellation method, was proposed on the basis of practical rail profile, material and operational noise. PLB was applied to simulate the AE of rail head crack. Field tests were carried out respectively to acquire the AE waves generated by PLBs at various propagation (source-sensor) distances and the operational noise caused by passing trains. WT was first utilized

to investigate the time-frequency characteristics of different AE sources and the dispersion phenomena of AE waves propagating along the rail head. Here, Shannon entropy of wavelet coefficients was used to select the optimal mother wavelet. Then, the WT-MAL method was applied to locate the AE sources (i.e., simulated cracks) respectively for the PLB-induced AE signals with and without operational noise. The group velocities of the two prominent dispersive wave modes used were experimentally determined. For those AE signals inundated with operational noise, the Hilbert transform (HT)-based noise cancellation method was employed to improve the signal-to-noise ratio (SNR). Finally, the results of source location and noise cancellation were discussed.

2. Experimental setup and data acquisition

PLB can produce uniform and stable AE sources, which have similar frequency components of rail crack-induced AE waves (Li *et al.* 2015), and is widely used by researchers to simulate the AE signal of rail crack (Zhang *et al.* 2015). In order to explore the propagation characteristics and source location of AE waves in rail head, the PLB test was conducted to acquire the AE waves generated by PLBs at various source-sensor distances. In order to study the influence of noise on source location and noise cancellation, the train pass-by test was done to record the operational noise caused by passing trains. The two kinds of AE signals were combined to simulate the actual AE events of rail head cracks in a typical noisy environment. Such a way of signal synthesis with random phase angles is commonly adopted by researchers to simulate actual cases under limited experimental conditions (Audoin *et al.* 2006, Hamstad and O'Gallagher 2005). The experimental setup and data acquisition procedure are introduced in this section.

2.1 Field PLB test

The PLB test was conducted on a rail track located in China during its non-operational periods without trains running. The setup is shown in Fig. 1. The rail track was 60 kg/m U71Mn rail, the cross-section and material of which were similar to those of the worldwide used UIC60 rail. The rail track was supported by concrete sleepers and ballast. The distance between two rails was 1435 mm, and the distance between two adjacent sleepers was 600 mm. According to the ASTM E976-10 (2010), a mechanical pencil with 2H leads of 0.5 mm diameter was utilized as the AE source in a reproducible way. The length of lead to be broken was 3 mm each time. A shoe was used to ensure that the leads break consistently at 30° angle.

As shown in Fig. 1, two AE sensors, S1 and S2, were installed at 30.0 m apart. The pencil leads were broken on the running surface of rail head at fourteen locations along the rail in order to record AE waves at various source-sensor distances. These locations, measured from S1, were 0.0 m, 0.5 m, 1.0 m, 2.5 m, 5.0 m, 10.0 m, 15.0 m, 20.0 m, 25.0 m, 30.0 m, 35.0 m, 40.0 m, 45.0 m and 50.0 m, as marked by the crosses. Four different sensor mounting positions on the rail cross-section were tested: top of rail head (P1), field side of rail head (P2), underside of rail head (P3), and middle of rail web (P4). For each sensor mounting position, PLBs were carried out successively at all the locations. At each location, a series of ten PLBs were done.

The amplitudes of PLB-induced AE waves at the four different mounting positions, P1-P4, were compared. For example, after the AE waves propagated 20.0 m along the rail head, the average amplitudes recorded by S1 at P1-P4 were respectively 0.52 V, 0.29 V, 0.073 V, and 0.052 V. It can be

concluded that the energy of AE waves arising from the rail head is mainly guided in the rail head when they propagate along the rail. Excluding P1, which is not practicable for continuous monitoring of operational railway, P2 is the optimal position for sensors to collect AE waves with less attenuation than P3 and P4. More importantly, the dispersion phenomena of AE waves in the rail head would be clearly observed by sensors at P2. While, it was found that if an AE source arose from the rail web or foot, the signals received by sensors at P2 would not contain any obvious dispersive wave modes. Thus, AE sensors are recommended to be mounted at P2 for the crack detection of rail head. The AE waves discussed in the following sections are all obtained by sensors mounted at P2.

2.2 Field train pass-by test

The train pass-by test was carried out on the same rail track during its operational periods with trains running. The setup is shown in Fig. 2. Sensors were installed on the field side of rail head (P2) as results from the PLB test showed P2 to be the optimal position for rail head crack detection. The operational noise was recorded during the passing of two trains: a fully loaded passenger train with axial load of about 17,000 kg running at approximately 120 km/h, and an empty passenger train with axial load of about 12,000 kg ran at approximately 80 km/h.

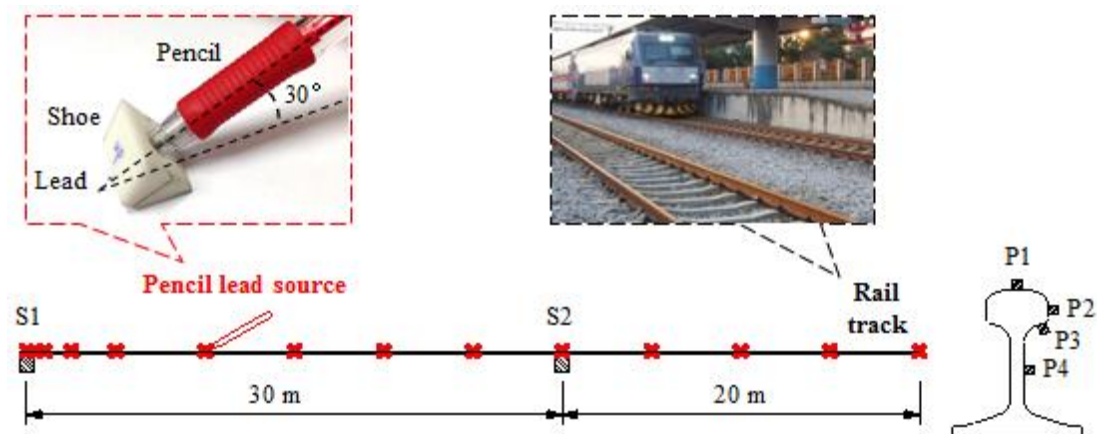


Fig. 1 Setup of PLB test

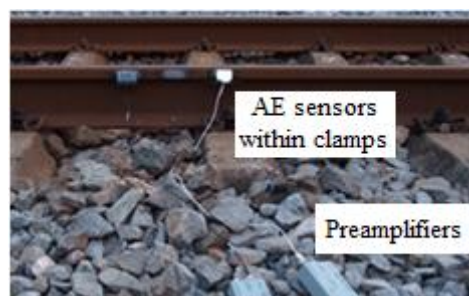


Fig. 2 Setup of train pass-by test

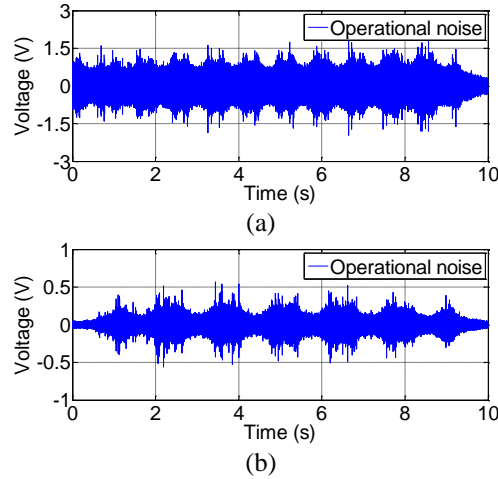


Fig. 3 Operational noise in train pass-by test (a) a full loaded train and (b) an empty train

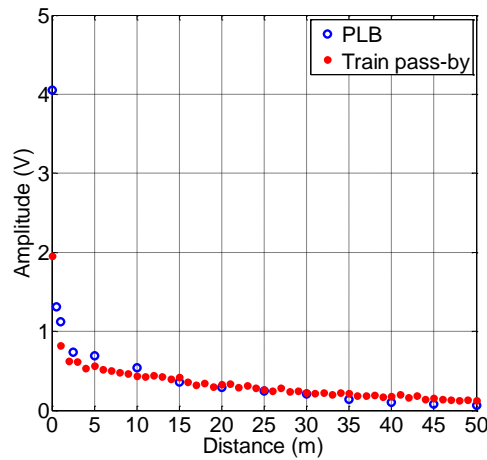


Fig. 4 Amplitude attenuation of PLB-induced AE waves and operational noise

The energy of the operational noise highly depends on the speed and axle load of train. Fig. 3(a) shows a 10-s segment of operational noise continuously recorded during the passing of a fully loaded passenger train. Fig. 3(b) shows another one recorded during the passing of an empty passenger train. Due to higher train speed and axle load, the operational noise in Fig. 3(a) with peak amplitude of about 1.86 V is much higher than that in Fig. 3(b) with peak amplitude of about 0.57 V. To test the robustness of the proposed crack detection strategy, the higher operational noise will be used in the following analysis.

2.3 AE data acquisition system

Two types of AE sensors supplied by Physical Acoustics were used. Micro80D sensors have a wide operating bandwidth of 175-900 kHz with a resonant frequency of around 325 kHz. They are small, and hence could be installed on the rail head for crack detection more conveniently with minimal intrusiveness. F50 α sensors have a wide operating bandwidth of 200-800 kHz with a resonant frequency of around 270 kHz. They have a flat frequency response over the operating bandwidth, and were used here, as a comparison with Micro80D sensors, to explore the natural frequency characteristics of AE sources more accurately. The AE data presented in this paper, if not specified, were captured using Micro80D sensors.

Adhesive couplant was applied to ensure good contact between sensor and rail surface. Magnetic clamps were utilized to fix them in place. AE signals acquired by the sensors were amplified via preamplifiers and finally recorded by the data acquisition board. For all the tests, the gain of preamplifier was set to 40 dB, the sampling rate was 5 MHz, and the analog band-pass filter was 100-1000 kHz.

2.4 Amplitude attenuation of AE waves

To be effective in the rail crack monitoring, the sensing distance of AE sensors should be as long as possible. It was therefore of interest to examine the expected attenuation of AE waves along rail head. Fig. 4 displays the attenuation trends of both PLB-induced AE waves and operational noise propagating along the rail head. As the propagation distance increased from 0.0 m to 50.0 m, the peak amplitudes of PLB-induced AE waves recorded varied from 4.05 V to 0.016 V, and those of AE noise generated by the passing train varied from 1.95 V to 0.12 V. In general, the AE wave induced by PLB exhibits a steeper attenuation compared to the operational noise. This is not surprising since PLB is a single-hit event, while a passing train is a continuously moving source. However, both types of the AE waves undergo steep decays initially followed by more gradual decreases.

3. Crack detection strategy

The crack detection strategy proposed in this paper focuses on source location and noise cancellation. AE signal in the field contains the information of both crack and operational noise. It should be denoised using an analog filter or the HT-based numerical method. After that, only AE segments of high amplitudes above the pre-set threshold will be considered as the crack-induced AE hits and saved to computer for crack location analysis by the WTMAL method. A flowchart of this crack detection strategy is summarized in Fig. 5. The details of WT, WTMAL source location method and HT-based noise cancellation method are introduced in this section.

3.1 WT and optimal mother wavelet selection

AE waves are non-stationary signals whose power spectra change with time. WT is a powerful tool that has been applied to characterize them fully in the time-frequency domain (Hamstad *et al.* 2002, Suzuki *et al.* 1996). Instead of discrete wavelet transform (DWT), continuous wavelet transform (CWT) is implemented in this study as it operates in more detailed scales, provides more

powerful multi-resolution capability, and performs better in singularity detection of noisy data. CWT is defined as the convolution of signal $x(t)$ to be analyzed and a series of wavelet functions $\psi_{a,b}(t)$ which are simply dilated and translated from a unique admissible mother wavelet $\psi(t)$ (Teolis 1998).

$$WT(a,b) = \int_{-\infty}^{\infty} x(t)\psi_{a,b}^*(t)dt = \frac{1}{\sqrt{a}} \int_{-\infty}^{\infty} x(t)\psi^*\left(\frac{t-b}{a}\right) dt \tag{1}$$

Here, $(\cdot)^*$ denotes the complex conjugate, $a > 0$ is the scale parameter, b is the translation parameter, t is time, and $WT(a,b)$ is the corresponding wavelet coefficient. The wavelet function $\psi_{a,b}(t)$ is centered at b with a spread proportional to a , and could be regarded as a window function in both of the time and frequency domains. During the transform, a series of $\psi_{a,b}(t)$ is generated according to variable values of a and b . By such an approach, time-frequency localization analysis is realized.

The choice of mother wavelet has a significant influence on the results of WT. A suitable mother wavelet should be selected by taking into account the properties of the wavelets (e.g., symmetry, orthogonality, and support size) and the AE waves of interest. In this study, complex Morlet wavelet is selected as it provides excellent resolution in both of the time and frequency domains (Ciampa and Meo 2010, Zhang *et al.* 2014). Its function and corresponding Fourier transform are, respectively

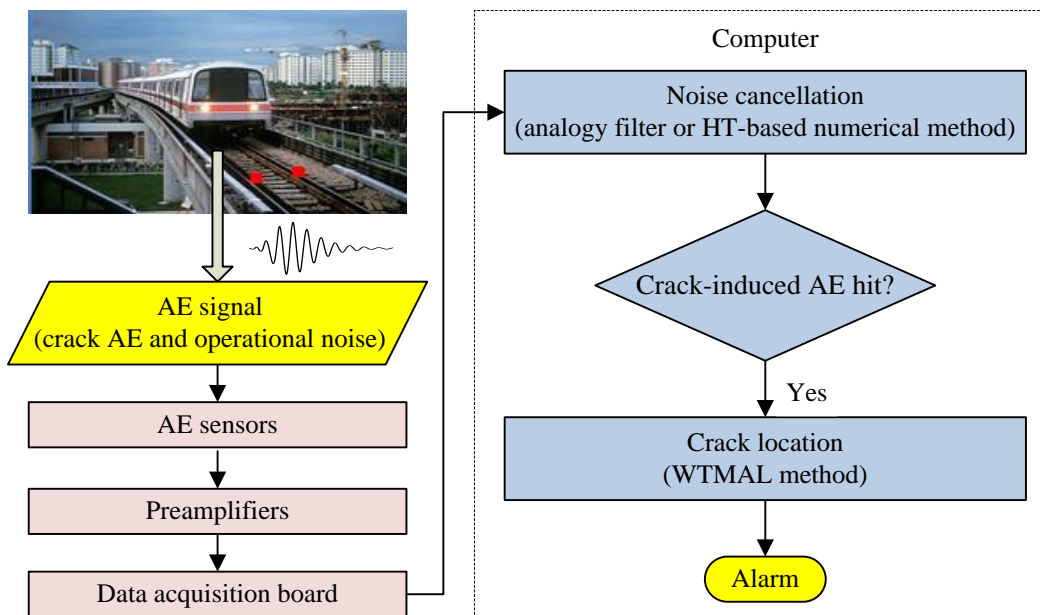


Fig. 5 Flowchart of the crack detection strategy proposed in this study

$$\psi(t) = \frac{1}{\sqrt{\pi f_b}} \exp(i2\pi f_c t) \exp\left(-\frac{t^2}{f_b}\right) \quad (2)$$

$$\hat{\psi}(f) = \exp\left\{-\pi^2 f_b (f - f_c)^2\right\} \quad (3)$$

and i is the imaginary unit. For practical applications, it is considered admissible for $2\pi f_c \geq 5$ because of the fast decay of its envelope towards zero (Teolis 1998).

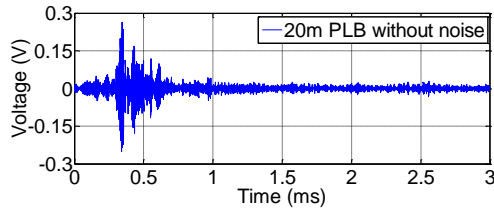
The Shannon entropy of wavelet coefficients (He *et al.* 2008) is then utilized as a quantitative criterion to select the optimal mother wavelet with appropriate parameters. Low Shannon entropy indicates high diversity of the wavelet coefficient matrix, which corresponds to high energy concentration. Thus, an optimal mother wavelet would produce a wavelet coefficient matrix of the minimum Shannon entropy. Assuming that $w_{t_{ij}}$ ($i=1,2,\dots,N$, $j=1,2,\dots,M$) is a set of wavelet coefficients, its Shannon entropy is defined as

$$S_{WT} = -\sum_{i=1}^N \sum_{j=1}^M p_{ij} \log p_{ij} \quad \text{where} \quad p_{ij} = \frac{|w_{t_{ij}}|^2}{\sum_{i=1}^N \sum_{j=1}^M |w_{t_{ij}}|^2} \quad (4)$$

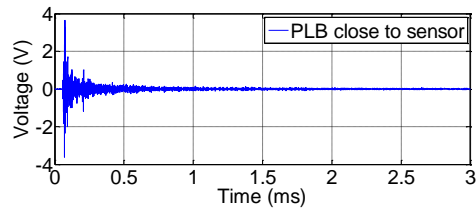
It is noted that $\sum_{i=1}^N \sum_{j=1}^M p_{ij} = 1$, and $p_{ij} \log p_{ij} = 0$ if $p_{ij} = 0$. Using a number of experimental AE signals, the Shannon entropy values were calculated for complex Morlet mother wavelets with various f_b and f_c . Finally, the optimal mother wavelet was found to be the one with $f_b = 0.5$ and $f_c = 4$ Hz. As an example, the entropy calculation results for a crack-induced AE wave are listed in Table 1. It is shown that the optimal mother wavelet leads to the lowest wavelet entropy value 4.416.

Table 1 Entropy calculation results of various mother wavelets

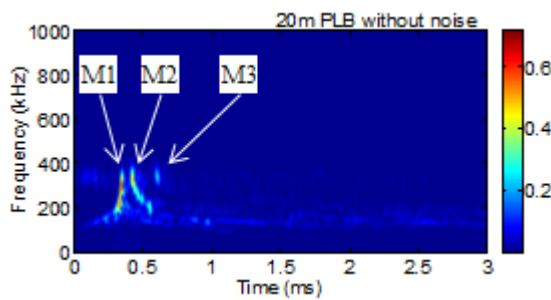
Complex Morlet f_b (non-dimensional)	Complex Morlet f_c (Hz)						
	1	2	3	4	5	6	7
0.1	5.061	4.786	4.613	4.525	4.475	4.446	4.431
0.5	4.732	4.496	4.429	4.416	4.428	4.447	4.467
1	4.594	4.435	4.417	4.437	4.466	4.495	4.518
3	4.454	4.423	4.469	4.512	4.546	4.573	4.594
5	4.423	4.448	4.507	4.549	4.581	4.606	4.627
10	4.417	4.497	4.557	4.595	4.625	4.652	4.674
15	4.431	4.527	4.584	4.621	4.652	4.679	4.702
20	4.447	4.548	4.602	4.640	4.672	4.699	4.722



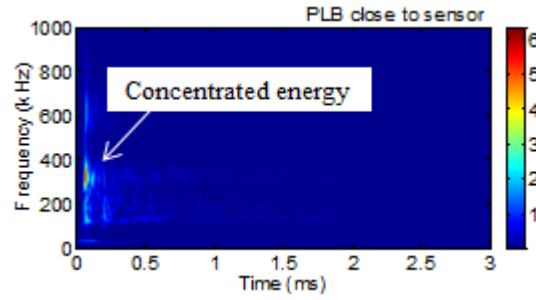
(a)



(a)



(b)



(b)

Fig. 6 Dispersive modes of an AE wave in rail head with propagation distance of 20.0 m: (a) waveform and (b) WT

Fig. 7 An AE wave in rail head with the source very close to the sensor: (a) waveform and (b) WT

3.2 Dispersion of AE waves in rail head

The AE wave should be regarded as guided wave when propagating along the rail head, a beam-like structure. One of the key characteristics of guided wave is velocity dispersion. That is, different frequency components travel through a media at different velocities, depending on the material density and elastic constant, structural thickness, and wave frequency (or wavelength). Because of the irregular cross-section of rail track, it is difficult to apply the Rayleigh-Lamb equation to determine the dispersive wave modes and their group velocities in rail head (Coccia *et al.* 2011, Zhang *et al.* 2014). This is further complicated by the frequency components of AE source, frequency response of AE sensor and multiple reflections from structural boundaries. Thus, the dispersion phenomena of AE waves propagating in rail head were experimentally examined in this study. As an example, Fig. 6 shows the WT spectrum of an AE wave with propagation distance of 20.0 m. Three dispersive wave modes, respectively named M1, M2, and M3, are clearly observed. However, if the propagation path is too short, it would be difficult for the wave modes to be distinguished from one another due to the time resolution limit of data acquisition and the effect of local wave reflection. Fig. 7 shows the WT spectrum of another AE wave with propagation distance of less than 0.1 m. The concentrated wave energy shows no distinct dispersion indicating that the AE source is very close to the sensor.

3.3 WTMAI source location method

3.3.1 Preparatory works of WTMAI method

Before applying the WTMAI method to locate an AE source, three preparatory works should be done in advance, respectively wave modes selection, scale selection and group velocity determination of wave modes. Firstly, two appropriate wave modes are selected as the objectives. WT is performed on AE wave as shown in Fig. 6, whereby M1 and M2 are proposed because their prominent magnitudes make them to be identified easily.

Secondly, the wavelet coefficients corresponding to a certain scale, i.e., frequency, are extracted, where the peaks indicate the arrival times of selected wave modes travelling with different group velocities. An appropriate scale is selected where the wave modes concerned are typically present with high energy and clearly separated with each other. In this study, wavelet coefficients of the scale nearest to 300 kHz are extracted, and their squared values (also known as wavelet power) are plotted in order to accentuate the divergence (Fig. 8). The two main peaks having the highest amplitudes are identified as M1 and M2 respectively.

Thirdly, the group velocities of selected wave modes are experimentally determined using a pair of sensors attached along the rail head, labelled as S1 and S2 as shown in Fig. 9. The distance between the two sensors is denoted by d_0 , and the distances between AE source and the sensors are respectively d_1 and d_2 . Let the arrival times of M1 at the two sensors be $t_{1,1}$ and $t_{1,2}$, and those of M2 be $t_{2,1}$ and $t_{2,2}$. Then their group velocities, V_1 and V_2 , are obtained

$$V_1 = \frac{d_2 - d_1}{t_{1,2} - t_{1,1}} \quad \text{and} \quad V_2 = \frac{d_2 - d_1}{t_{2,2} - t_{2,1}} \quad (5)$$

3.3.2 Application of WTMAI method

After all the preparatory works done ahead, the cracks, i.e., AE sources, can be located using the WTMAI method. The distance d from AE source to a sensor, named target sensor, is calculated based on the temporal separation of the two selected wave modes and their group velocities

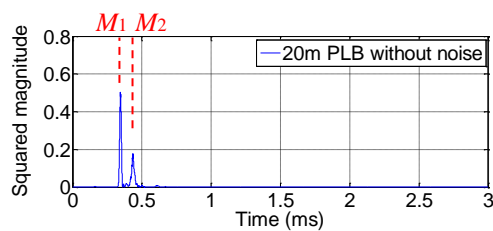


Fig. 8 Squared wavelet coefficients at 300 kHz of an AE wave in rail head with propagation distance of 20.0 m

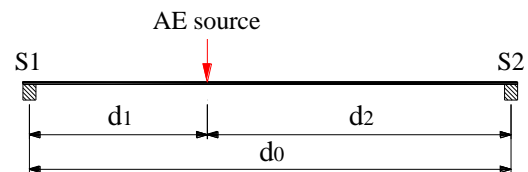


Fig. 9 Principle of group velocity determination

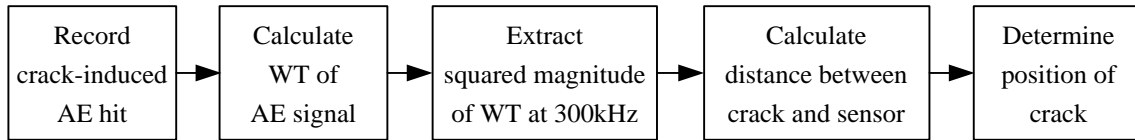


Fig. 10 Flowchart of crack location in rail head using WTMAL method

$$d = (t_2 - t_1) \left(\frac{V_1 V_2}{V_1 - V_2} \right) \quad (6)$$

where t_1 and t_2 are the arrival times of M1 and M2 at the target sensor. It should be noted that only the target sensor is needed for the purpose of distance calculation. The final location will then be identified with the help of its two neighbouring sensors on both sides. If the upstream sensor records the same AE event as the target sensor, the detected AE source should be on the upstream side of target sensor, and vice versa. A flowchart for the field application of WTMAL method is summarized in Fig. 10.

3.3.3 Blind zone and working range of AE sensor

As highlighted earlier, if the distance between AE source and sensor is too short, the dispersion of wave modes would be too indistinct to be detected. Thus, in the WTMAL method, a specific distance from the AE sensor is considered as its blind zone, beyond which lies its working range. Another reason of blind zone is that source location is made more difficult in the case of field rail track with high operational noise. Based on the field tests, it is found that when a train wheel is passing nearby, the target sensor can not identify a crack-induced AE wave arising from a long distance away, because the wave energy has been significantly attenuated and become too weak relative to the train wheel-induced noise. Even a filter with a very high high-pass cutoff frequency does not help. The sensor will become ineffective if there is a train wheel running in its blind zone. However, this blind zone problem can be addressed by the cooperation between neighbouring sensors. Along the rail, sensors could be arranged in a way that the blind zone of a sensor is monitored by its neighbouring sensors and vice versa. Then, the working ranges of all AE sensors collectively cover the entire rail length of interest without any blind zone. The distance between neighbouring sensors will be determined finally depending on the experimental results.

3.4 Hilbert transform-based noise cancellation method

Due to the high operational noise encountered in the railway system, noise cancellation is important in order to improve the SNR and to detect crack-induced AE hits of interest through a threshold of waveform amplitude. The operating frequency bands of AE sensor and analog filter could be properly selected during data acquisition. However, digital denoising is still valuable in view of its convenience in post-processing of AE signal. In this paper, a new noise cancellation method based on HT is employed to filter out those noise-related frequency components so as to determine the appropriate value of cutoff frequency for field application.

Recently, Chen and Wang (Chen and Wang 2012, Wang *et al.* 2015) formulated a signal

decomposition theorem based on HT to accurately separate a finite bandwidth signal into a series of narrow band components. Feldman (Feldman 2011) further proposed to apply it as a zero-phase digital filter. The HT of a signal $x(t)$ is defined as the convolution integral of $x(t)$ with $(\pi t)^{-1}$:

$$HT[x(t)] = \tilde{x}(t) = \frac{1}{\pi} \int_{-\infty}^{\infty} \frac{x(\tau)}{t - \tau} d\tau \quad (7)$$

Physically, the HT is equivalent to a kind of linear filter, where all the amplitudes of spectral components are left unchanged, but their phases are shifted by $-\pi/2$ (Feldman 2011). The signal $x(t)$ is assumed to comprise relative slow components $s(t)$ and fast components $f(t)$ with non-overlapping spectra. A complex function $Y(t) = y(t) + i\tilde{y}(t)$ is introduced that has an intermediate spectrum between the spectra of $s(t)$ and $f(t)$. Here $\tilde{y}(t)$ is the HT of $y(t)$, and $y^2(t) + \tilde{y}^2(t) = 1$. For a constant cutoff frequency ω_c , $Y(t) = \cos \omega_c t + i \sin \omega_c t$. Then the low frequency components $s(t)$ and high frequency components $f(t)$ can be obtained through

$$\begin{cases} s(t) = HT[x(t)\cos \omega_c t] \sin \omega_c t - HT[x(t)\sin \omega_c t] \cos \omega_c t \\ f(t) = x(t) - s(t) \end{cases} \quad (8)$$

Eq. (8) is regarded as a zero-phase digital filter that preserves the initial amplitude, frequency and phase relations of extracted components. The cutoff frequency could even be a function of time. Significantly, based only on the forward Hilbert transform, it is easier to be implemented than the filtering techniques based on wavelet packet and wavelet transform, and hence provides a new noise cancellation approach for AE signals of high non-stationarity. Fig. 11 reveals the concept of HT-based noise cancellation method for rail crack detection, where the block diagram of digital filter is included. The energy of rail operational noise, considered as $s(t)$, is predominantly focused in relatively lower frequency range than that of crack-induced AE signal, considered as $f(t)$. A two-stage filtering process is designed in order to eliminate the aliasing and phase reversal due to discretization of signal. Through an appropriate cutoff frequency ω_c , the SNR of AE signals inundated with noise could be greatly improved.

4. Results and discussions

4.1 Time-frequency characteristics of AE waves

The time-frequency characteristics of AE waves induced by PLB and operational noise, and the effect of frequency response of sensors on those AE waves were analyzed through WT. Fig. 12 presents the waveform and WT of a PLB-induced AE wave recorded by an F50 α sensor. The wave energy is distributed mainly in the range of 100 - 250 kHz with a peak at approximately 120 kHz. There is also a notable portion of energy in the high frequency range of 450 - 600 kHz. Fig. 14 presents the waveform and WT of a segment of operational noise recorded by an F50 α sensor. Markedly different from the PLB-induced AE wave, the operational noise caused by passing trains has energy contents clustering predominantly below 180 kHz, although the corresponding

sensitivity coefficients of AE sensor are very low. Fig. 13 shows another PLB induced AE wave recorded by a Micro80D sensor, while Fig. 15 shows the operational noise recorded by a Micro80D sensor at the same time as that of Fig. 14. Affected by the frequency response of Micro80D sensor, the PLB-induced AE wave recorded has energy contents mainly concentrated in the range of 100-400 kHz with a peak at approximately 300 kHz.

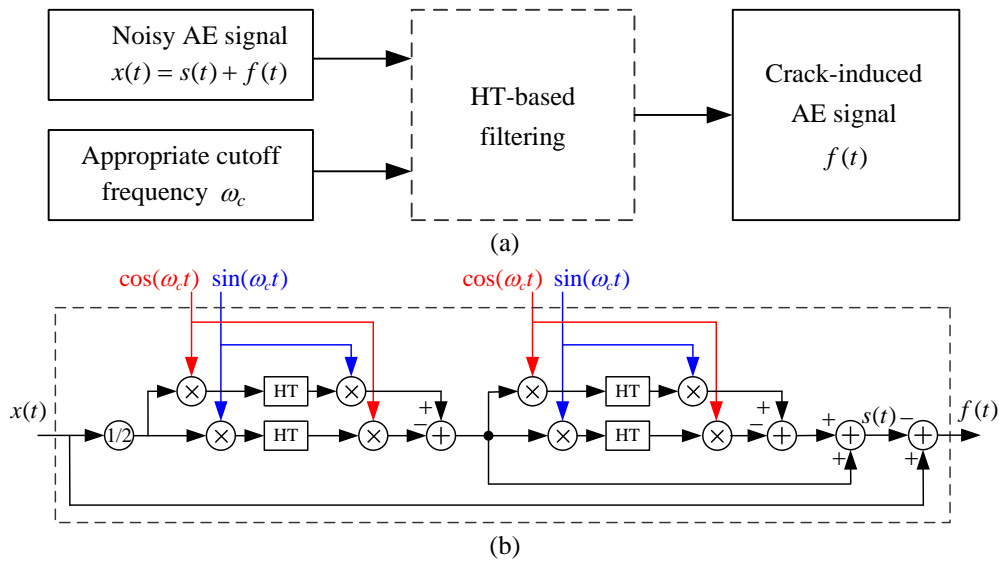


Fig. 11 HT-based noise cancellation method: (a) flowchart of concept and (b) block diagram of HT-based digital filter

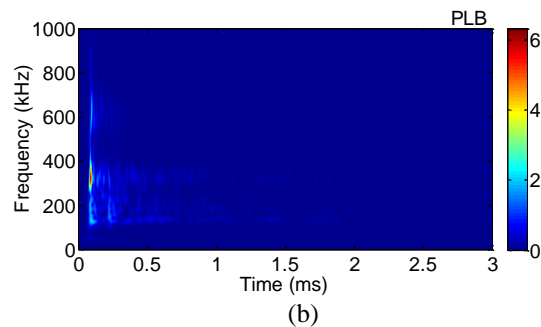
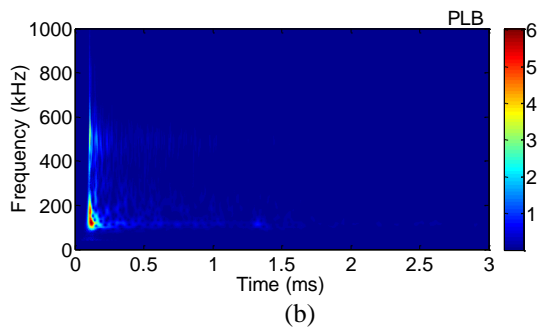
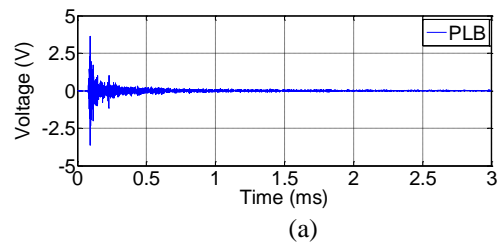
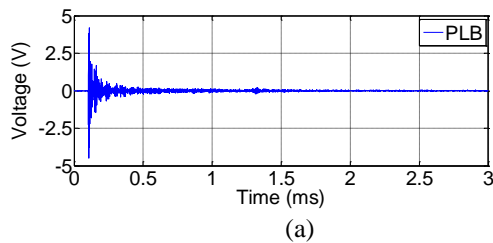


Fig. 12 A PLB-induced AE wave recorded by an F50α sensor: (a) waveform and (b) WT

Fig. 13 A PLB-induced AE wave recorded by a Micro80D sensor: (a) waveform and (b) WT

However, it is observed that the operational noise recorded by the Micro80D sensor still has energy contents clustering predominantly below 180 kHz, as the same as that recorded by the F50 α sensor. Overall, although F50 α helps to explore the natural frequency characteristics of different AE sources more accurately, Micro80D sensor is more suitable for field rail crack detection. Because the PLB-induced AE signal recorded by Micro80D sensor is distinguished more readily from the operational noise-induced AE signal, in the view of their energy concentration ranges. By filtering out the lower frequency components of AE signal, the influence of noise can be greatly reduced.

4.2 Source location without operational noise

The WT of PLB-induced AE waves without operational noise were computed. The plots of waveform, WT and squared wavelet coefficients at 300 kHz for AE waves recorded by S1 with propagation distances 2.5 m, 10.0 m, 30.0 m and 40.0 m are shown in Figs. 16-19. Those for the case of 20.0 m have already been presented in Figs. 4 and 6. As can be seen, the two selected wave modes produce two main distinct peaks in the squared wavelet coefficients plots. The highest peak is induced by M1, and the second highest peak is by M2, of which the amplitude is generally above 20% of that of M1.

As the preparatory work, the group velocities of dispersive wave modes M1 and M2 in rail head were determined according to Eq. (5) using the PLBs data of S1 and S2, as shown in Table 2.

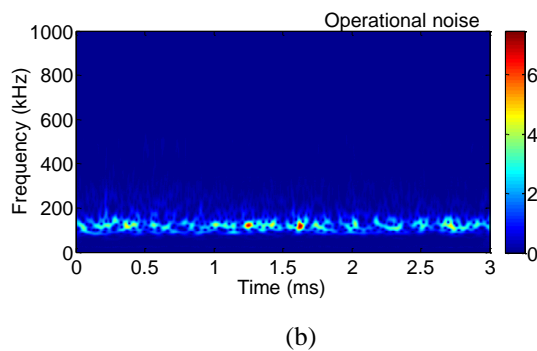
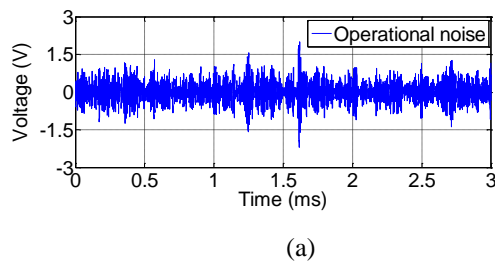


Fig. 14 Operational noise recorded by an F50 α sensor: (a) waveform and (b) WT

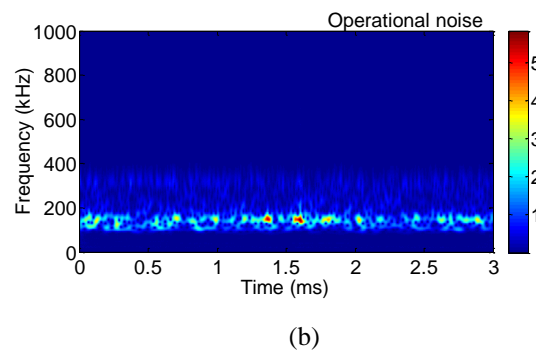
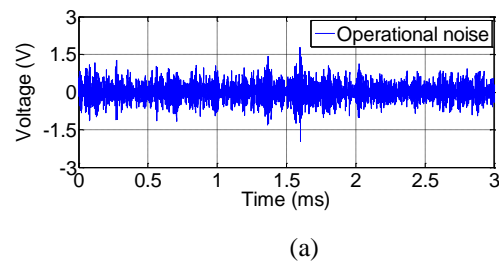


Fig. 15 Operational noise recorded by a Micro80D sensor: (a) waveform and (b) WT

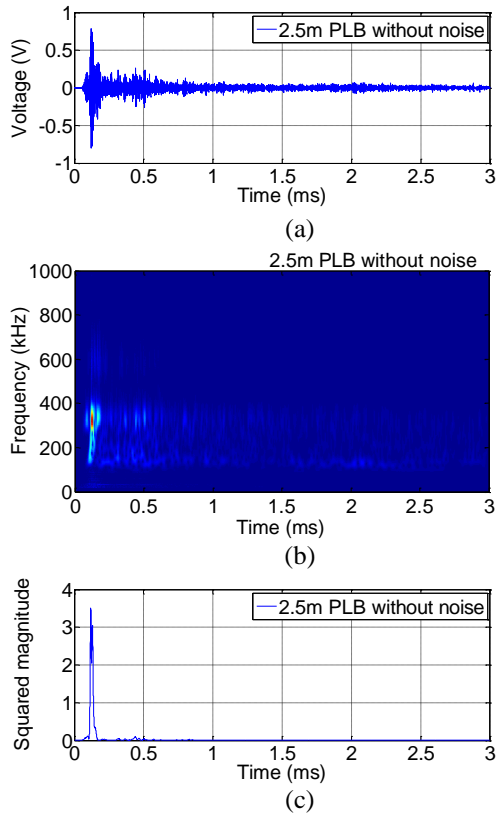


Fig. 16 PLB at 2.5 m without operational noise: (a) waveform, (b) WT and (c) squared wavelet coefficients at 300 kHz

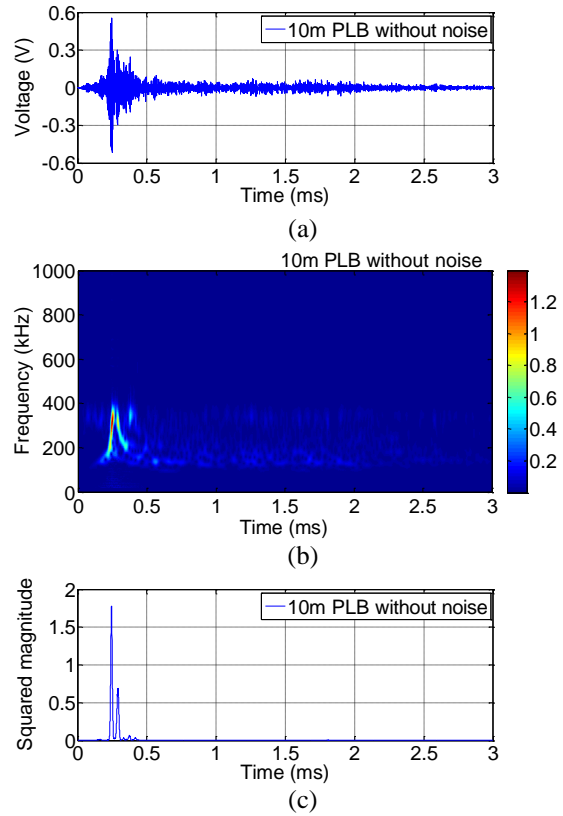


Fig. 17 PLB at 10.0 m without operational noise: (a) denoised waveform, (b) WT and (c) squared wavelet coefficients at 300 kHz

The velocities in each case of propagation distance are the average results of ten PLBs. The results of all the cases are further averaged to obtain the final two group velocities at 300 kHz, respectively 2960.15 m/s and 2920.50 m/s with standard deviations below 2.00 m/s. As indicated previously, due to the short propagation distance, the two wave modes could not be identified at 0.0 m, 0.5 m and 1.0 m. In the case of 15.0 m, Eq. (5) does not yield a solution because $d_2 - d_1 = 0$.

Besides, when the propagation distance is longer than 40.0 m, the energies of wave modes, especially M2, become too weak to be clearly identified in the WT. Based on these observations, the blind zone of a single AE sensor is preliminarily defined to be within 2.5 m, and the working range of the sensor alone is then to be from 2.5 to 40.0 m on each side when using WTMAL method. Considering the cooperation between neighbouring sensors, the average working range of each sensor is 40.0 m.

Taking S1 as the target sensor, the AE sources were located by the WTMAL method for PLB-induced AE waves in its working range. The time differences of wave modes, $t_2 - t_1$, were extracted. Based on the experimentally determined group velocities, the distances between various AE sources and the sensor were computed according to Eq. (6). As tabulated in Table 3, the

proposed source location method successfully locate the AE sources with errors of less than ± 0.30 m along the rail head when there is no operational noise.

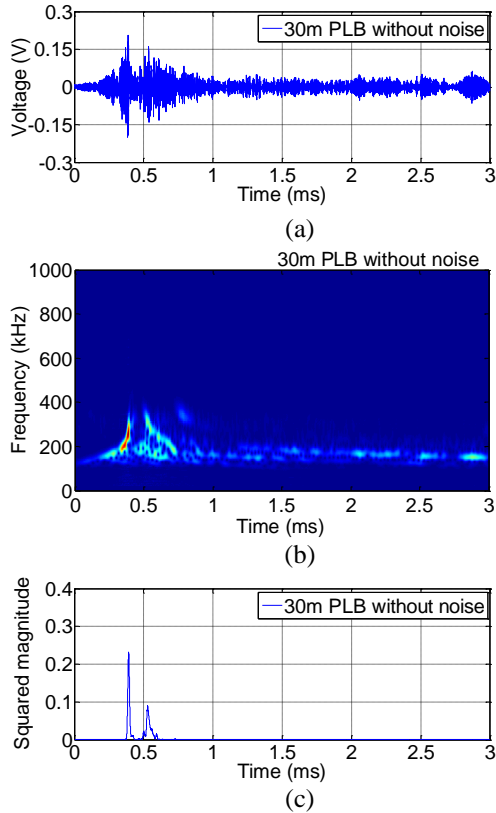


Fig. 18 PLB at 30.0 m without operational noise: (a) denoised waveform, (b) WT and (c) squared wavelet coefficients at 300 kHz

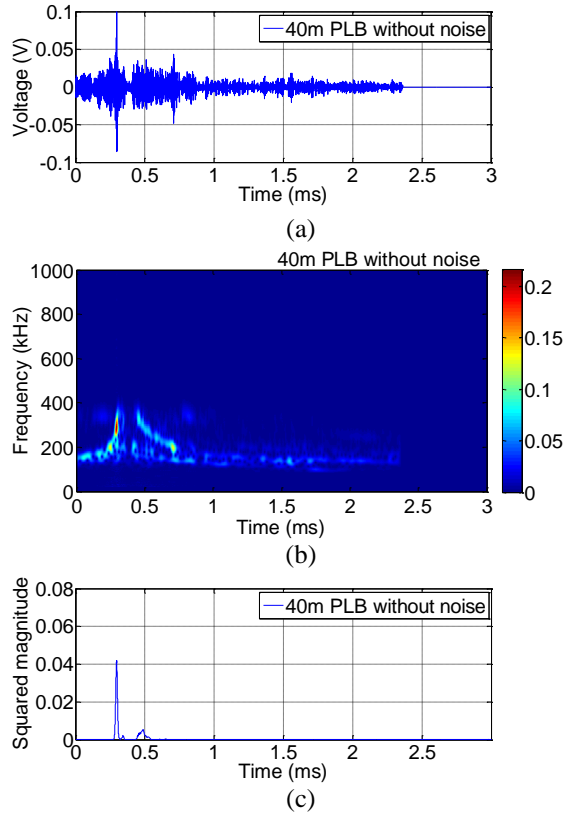


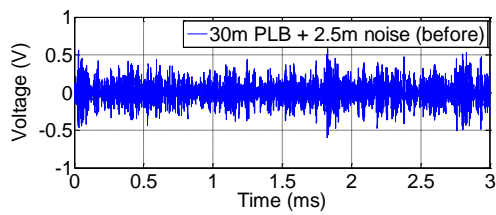
Fig. 19 PLB at 40.0 m without operational noise: (a) waveform, (b) WT and (c) squared wavelet coefficients at 300 kHz

Table 2 Group velocity determination results

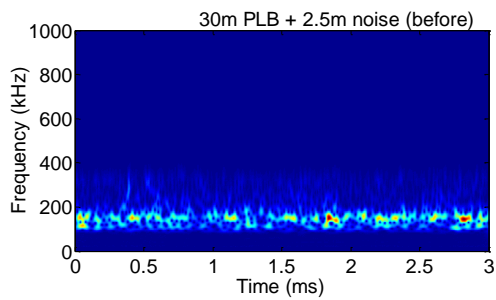
Propagation distance	V_1	Mean	Standard deviation	V_2	Mean	Standard deviation
	(m/s)			(m/s)		
2.5 m	2958.25			2919.42		
5.0 m	2959.81			2919.95		
10.0 m	2960.95			2921.56		
20.0 m	2961.24	2960.15	1.23	2919.88	2920.50	1.50
25.0 m	2958.97			2918.43		
30.0 m	2961.57			2922.50		
35.0 m	2959.32			2919.79		
40.0 m	2961.12			2922.47		

Table 3 Source location results of PLB simulated AE waves with and without operational noise

Propagation distance	Without noise			With noise		
	$t_2 - t_1$ (μs)	Identified d (m)	Absolute error (m)	$t_2 - t_1$ (μs)	Identified d (m)	Absolute error (m)
2.5 m	12.0	2.62	0.12	12.0	2.62	0.12
5.0 m	23.4	5.10	0.10	23.4	5.10	0.10
10.0 m	47.0	10.25	0.25	47.2	10.29	0.29
15.0 m	67.8	14.78	0.22	67.6	14.73	0.27
20.0 m	90.6	19.75	0.25	90.6	19.75	0.25
25.0 m	113.8	24.81	0.19	113.8	24.80	0.20
30.0 m	138.6	30.22	0.22	138.8	30.25	0.25
35.0 m	161.8	35.28	0.28	--	--	--
40.0 m	184.8	40.29	0.29	--	--	--

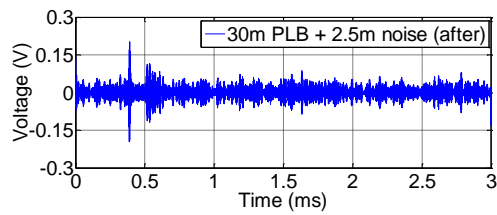


(a)

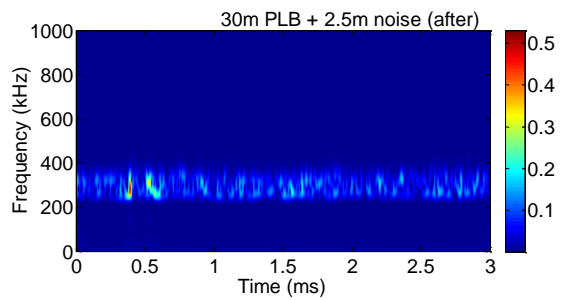


(b)

Fig. 20 AE signal combined by PLB-induced AE wave after propagating 30.0 m and operational noise at 2.5 m away from the wheel-rail contact point (before denoising): (a) waveform and (b) WT



(a)

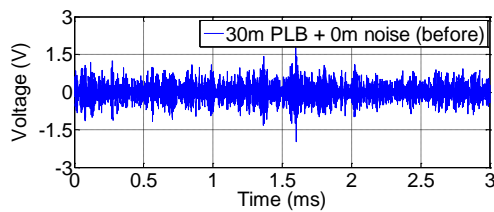


(b)

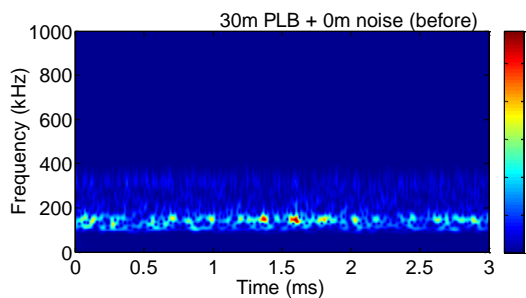
Fig. 21 AE signal combined by PLB-induced AE wave after propagating 30.0 m and operational noise at 2.5 m away from the wheel-rail contact point (after denoising): (a) waveform and (b) WT

4.3 Influence of operational noise on crack detection

The PLB-induced AE waves and operational noise were combined to simulate the actual cases of rail head cracks in a typical noisy environment. It was of interest to first investigate the influence of operational noise on the capability of the proposed noise cancellation and source location methods. After defining the blind zone of 2.5 m, a segment of operational noise that is 2.5 m away from wheel-rail contact point (a small segment from Fig. 3(a) with peak amplitude of 0.62 V) was selected and combined with those PLB-induced AE waves. Based on the previous time-frequency analysis, the HT-based noise cancellation method with a high-pass cutoff of 250 kHz was applied to filter out the lower frequency components associated with operational noise. Figs. 20 and 21 show the combined AE signals of 30.0 m case before and after denoising respectively. Before denoising, the combined signal is inundated with operational noise. The PLB-related features in both of the time and time-frequency domains only become prominent after denoising. The HT-based filter is demonstrated to be an effective noise cancellation method that greatly improves the SNR of AE signals. For a practical condition monitoring system, a 250 kHz high-pass analog filter can be used in order to detect crack-induced AE hits easily through an amplitude threshold in time domain. Moreover, even after denoising, the energies of PLB-induced AE wave after propagating more than 30.0 m and noise at 2.5 m away from the wheel-rail contact point are comparative. The average working range of each AE sensor is thus reduced from 40.0 m to 30.0 m due to the influence of operational noise.

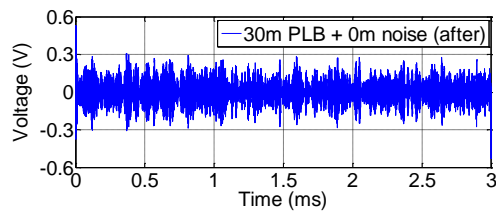


(a)

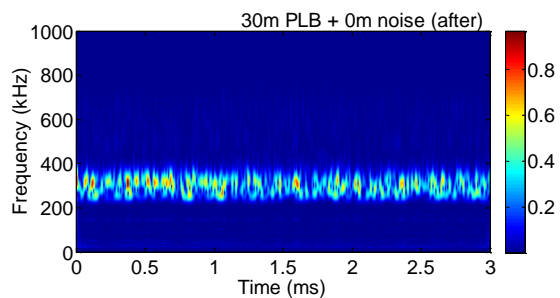


(b)

Fig. 22 AE signal combined by PLB-induced AE wave after propagating 30.0 m and operational noise at the wheel-rail contact point (before denoising): (a) waveform and (b) WT



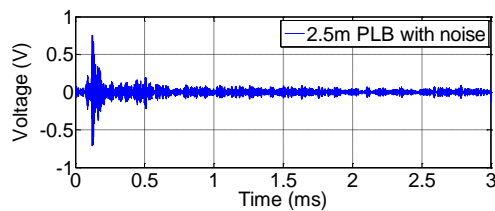
(a)



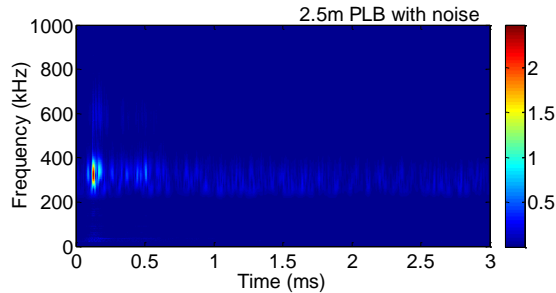
(b)

Fig. 23 AE signal combined by PLB-induced AE wave after propagating 30.0 m and operational noise at the wheel-rail contact point (after denoising): (a) waveform and (b) WT

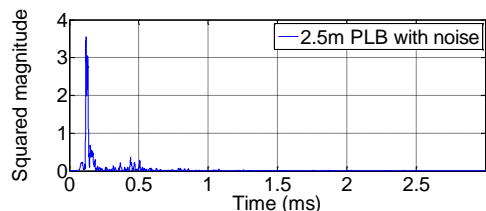
In addition, the high operational noise is another reason for defining a long blind zone of 2.5 m, besides of the wave dispersion as introduced in section 3.3. It is further illustrated here by the experimental results. Due to the small portion of wave energy of operational noise in the frequency range above 250 kHz, overlapping with that of PLB-induced AE wave, the SNR of denoised AE signal may still be low when the PLB-induced AE wave is too weak relative to operational noise, which is really strong at the wheel-rail contact point. One example is the situation where a wheel is passing near the sensor while a rail crack generates an AE wave at 30.0 m away stimulated by another wheel. The combined signals of the PLB-induced AE wave after propagating 30.0 m and the operational noise at the wheel-rail contact point (a small segment from Fig. 3(a) with peak amplitude of 1.95 V), are shown in Figs. 22 and 23, respectively before and after denoising. Unfortunately, even after denoising, it is still difficult to distinguish the PLB-induced AE wave from such high operational noise in either time domain or time-frequency domain. It indicates that the sensor would become ineffective when there is a train wheel running in its blind zone, even if a 250 kHz high-pass digital or analog filter is applied. Therefore, from the perspectives of both amplitude-threshold-trigger data acquisition of crack-induced AE hits and source location using WTMA method, a blind zone for a single AE sensor does exist in its adjacent distance.



(a)

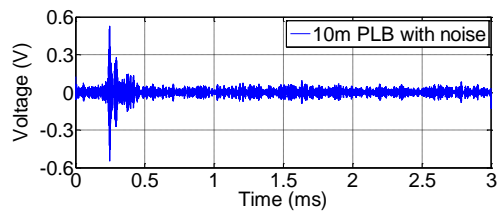


(b)

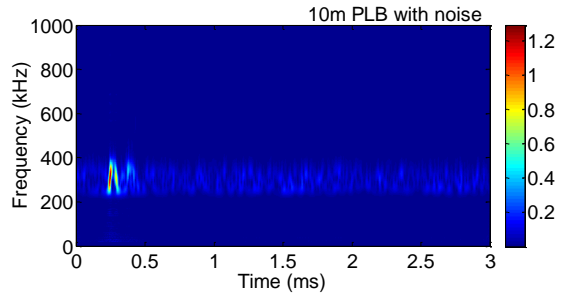


(c)

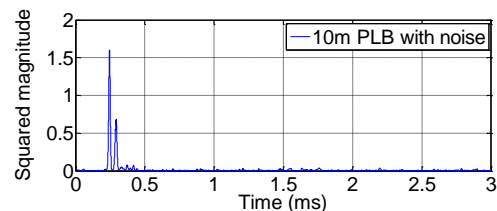
Fig. 24 PLB at 2.5 m with operational noise: (a) denoised waveform, (b) WT and (c) squared wavelet coefficients at 300 kHz



(a)

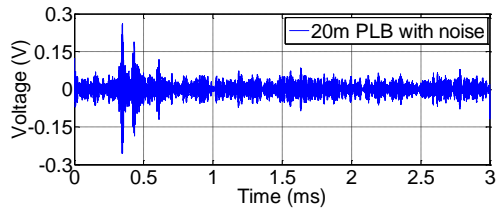


(b)

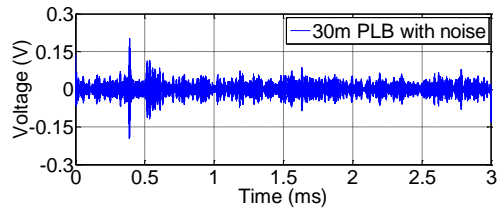


(c)

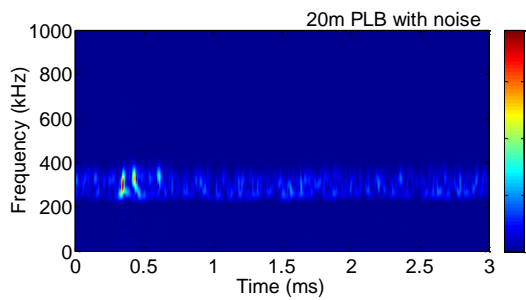
Fig. 25 PLB at 10.0 m with operational noise: (a) denoised waveform, (b) WT and (c) squared wavelet coefficients at 300 kHz



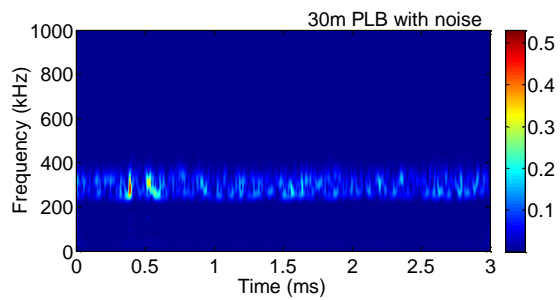
(a)



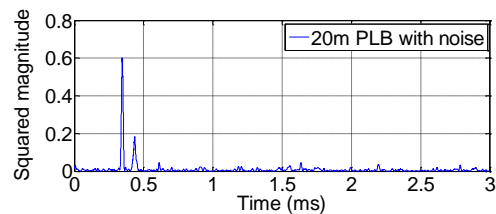
(a)



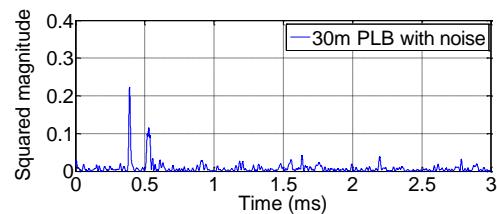
(b)



(b)



(c)



(c)

Fig. 26 PLB at 20.0 m with operational noise: (a) denoised waveform, (b) WT and (c) squared wavelet coefficients at 300 kHz

Fig. 27 PLB at 30.0 m with operational noise: (a) denoised waveform, (b) WT and (c) squared wavelet coefficients at 300 kHz

4.4 Source location with operational noise

The source location ability of the WTMAL method was further studied using the PLB-induced AE signals with operational noise. Here, a series of cases with PLB locations in the working range of the target sensor, S1, were investigated. After applying the HT-based filter with a high-pass cutoff frequency of 250 kHz, the waveforms, WTs and squared wavelet coefficients at 300 kHz of denoised AE waves were obtained. Those for cases of 2.5 m, 10.0 m, 20.0 m and 30.0 m are respectively shown in Figs. 24-27. The source location results of all the AE signals with operational noise are listed in Table 3 for comparison with those without operational noise. It is evident that even at high operational noise level the proposed source location method is still able to locate the AE sources with errors of less than ± 0.30 m along the rail head.

5. Conclusions

This study focuses on the crack detection in rail head, which is one of the most vulnerable parts of rail track, using AE technique. A crack detection strategy, including a source location method and a noise cancellation method, is proposed on the basis of practical rail profile, material and operational noise. The main findings are summarized below.

- The AE waves generated by PLBs at various propagation distances and the operational noise caused by passing trains were acquired separately through field tests. These two kinds of measured AE signals were combined to simulate the actual AE events of cracks in rail head with high operational noise.
- Through WT, the PLB-induced AE waves were observed to behave with obvious dispersion when propagating along the rail head. The operational noise was found to have energy mainly concentrated in a relatively lower frequency range than where PLB-induced AE waves operate. Here, the complex Morlet wavelet with $f_b = 0.5$ and $f_c = 4$ Hz was selected as the optimal mother wavelet by minimizing the Shannon entropy of wavelet coefficients.
- In order to locate the AE sources (i.e. simulated cracks), the WTMAL method was proposed, which makes use of the dispersion phenomena of AE waves in rail head and requires only one sensor to determine the distance between AE source and sensor. The group velocities of the two dispersive wave modes used at a selected scale were experimentally determined. For both of the PLB-induced AE signals with and without operational noise, the AE sources were located successfully with errors of less than ± 0.30 m along the rail head. The experimental results demonstrated the feasibility of the proposed source location method for field application even at high operational noise level.
- In order to identify crack-induced AE hits through an amplitude threshold in the presence of operational noise, a high-pass cutoff frequency of 250 kHz was recommended base on the experimental results. Although this denoising process could be achieved by an analog filter in the practical monitoring system, the HT-based noise cancellation method employed in this paper provides a new easy-to-use way to improve the SNR in AE signal processing.
- Given the WTMAL source location method used and the prevailing operational noise level detected, the average working range of each AE sensor reached 30.0 m. Although the sensing distance of sensors mounted on the track is relatively short compared to the length of railway lines, the crack detection strategy proposed can be applied to critical rail sections such as curved sections where lateral forces result in high occurrences of cracks.

Acknowledgments

This study was supported by the National University of Singapore Academic Research Fund (Grant No. R-302-000-097-112) and the National University of Singapore Research Scholarship. The authors would like to gratefully acknowledge the Wuhan Railway Bureau in China for providing access and assistance for the field tests.

References

- ASTM E976-10 (2010), *Standard Guide for Determining the Reproducibility of Acoustic Emission Sensor Response*, ASTM International, West Conshohocken, PA.
- Audoin, B., Pan, Y., Rossignol, C. and Chigarev, N. (2006), "On the use of laser-ultrasonics technique to excite selectively cylinder acoustic resonances", *Ultrasonics*, **44**, 1195-1198.
- Barke, D. and Chiu, W.K. (2005), "Structural health monitoring in the railway industry: a review", *Struct. Health Monit.*, **4**(1), 81-93.
- Bruzelius, K. and Mba, D. (2004), "An initial investigation on the potential applicability of Acoustic Emission to rail track fault detection", *NDT & E Int.*, **37**(7), 507-516.
- Chen, G.D. and Wang, Z.C. (2012), "A signal decomposition theorem with Hilbert transform and its application to narrowband time series with closely spaced frequency components", *Mech. Syst. Signal Pr.*, **28**, 258-279.
- Ciampa, F. and Meo, M. (2010), "Acoustic emission source localization and velocity determination of the fundamental mode A0 using wavelet analysis and a Newton-based optimization technique", *Smart Mater. Struct.*, **19**(4), 045027.
- Coccia, S., Bartoli, I., Marzani, A., Lanza di Scalea, F., Salamone, S. and Fateh, M. (2011), "Numerical and experimental study of guided waves for detection of defects in the rail head", *NDT & E Int.*, **44**(1), 93-100.
- Ernst, R. and Dual, J. (2014), "Acoustic emission localization in beams based on time reversed dispersion", *Ultrasonics*, **54**(6), 1522-1533.
- Esveld, C. (2001), *Modern Railway Track*, (2nd 2nd), MRT-Productions, Zaltbommel.
- Feldman, M. (2011), "Hilbert transform in vibration analysis", *Mech. Syst. Signal Pr.*, **25**(3), 735-802.
- Feldman, M. (2011), "A signal decomposition or lowpass filtering with Hilbert transform?", *Mech. Syst. Signal Pr.*, **25**(8), 3205-3208.
- Hamstad, M.A. and O'Gallagher, A. (2005), "Effects of noise on Lamb-mode acoustic-emission arrival times determined by wavelet transform", *J. Acoust. Emiss.*, **23**(1-24).
- Hamstad, M.A., O'Gallagher, A. and Gary, J. (2002), "A wavelet transform applied to acoustic emission signals: Part 2: Source location", *J. Acoust. Emiss.*, **20**, 62-82.
- He, Y., Yin, X. and Chu, F. (2008), "Modal analysis of rubbing acoustic emission for rotor-bearing system based on reassigned wavelet scalogram", *J. Vib. Acoust.*, **130**(6), 061009.
- Holford, K.M., Davies, A.W., Pullin, R. and Carter, D.C. (2001), "Damage location in steel bridges by acoustic emission", *J. Intel. Mat. Syst. Str.*, **12**(8), 567-576.
- Jiao, J., Wu, B. and He, C. (2008), "Acoustic emission source location methods using mode and frequency analysis", *Struct. Control Health.*, **15**(4), 642-651.
- Li, D., Kuang, K.S.C. and Koh, C.G. (2015), "Detection and quantification of fatigue cracks in rail steel using acoustic emission technique", *Structural Health Monitoring 2015, Proceedings of the 10th International Workshop on Structural Health Monitoring*, Stanford, CA, September.
- Li, S., Wang, X. and Zhao, M. (2015), "An improved cross-correlation method based on wavelet transform and energy feature extraction for pipeline leak detection", *Smart Struct. Syst.*, **16**(1), 213-222.
- Nair, A. and Cai, C.S. (2010), "Acoustic emission monitoring of bridges: Review and case studies", *Eng. Struct.*, **32**(6), 1704-1714.
- Ono, K. (2007), "Structural integrity evaluation using acoustic emission", *J. Acoust. Emiss.*, **25**, 1-20.
- Pandya, D.H., Upadhyay, S.H. and Harsha, S.P. (2013), "Fault diagnosis of rolling element bearing with intrinsic mode function of acoustic emission data using APF-KNN", *Expert Syst. Appl.*, **40**(10), 4137-4145.
- Papaelias, M.P., Roberts, C. and Davis, C.L. (2008), "A review on non-destructive evaluation of rails: state-of-the-art and future development", *P. I. Mech. Eng. F - J. Rai.*, **222**(4), 367-384.
- Suzuki, H., Kinjo, T., Hayashi, Y., Takemoto, M., Ono, K. and Hayashi, Y. (1996), "Wavelet transform of acoustic emission signals", *J. Acoust. Emiss.*, **14**(2), 69-84.
- Takemoto, M., Nishino, H. and Ono, K. (2000), Wavelet transform applications to AE signal analysis, in: T. Kishi, M. Ohtsu, S. Yuyama (Eds.) *Acoustic Emission-Beyond the Millennium*, Elsevier, Oxford, UK, pp.

35-56.

Teolis, A. (1998), *Computational Signal Processing with Wavelets*, Birkhäuser, Boston.

Thakkar, N.A., Steel, J.A. and Reuben, R.L. (2010), "Rail-wheel interaction monitoring using Acoustic Emission: A laboratory study of normal rolling signals with natural rail defects", *Mech. Syst. Signal Pr.*, **24**(1), 256-266.

Wang, Z.C., Geng, D., Ren, W.X., Chen, G.D. and Zhang, G.F. (2015), "Damage detection of nonlinear structures with analytical mode decomposition and Hilbert transform", *Smart Struct. Syst.*, **15**(1), 1-13.

Zhang, X., Feng, N., Wang, Y. and Shen, Y. (2014), "An analysis of the simulated acoustic emission sources with different propagation distances, types and depths for rail defect detection", *Appl. Acoust.*, **86**(0), 80-88.

Zhang, X., Feng, N., Wang, Y. and Shen, Y. (2015), "Acoustic emission detection of rail defect based on wavelet transform and Shannon entropy", *J. Sound Vib.*, **339**(419-432).

BS